Composite Structures 127 (2015) 426–435

Contents lists available at ScienceDirect

Composite Structures

journal homepage: www.elsevier.com/locate/compstruct

Perforation resistance of corrugated metallic sandwich plates filled with reactive powder concrete: Experiment and simulation

C.Y. Ni [a,b], R. Hou [a,b], H.Y. Xia [c,*], Q.C. Zhang [a,b], W.B. Wang [c], Z.H. Cheng [a,b], T.J. Lu [a,b]

[a] Multidisciplinary Research Center for Lightweight Structures and Materials, Xi'an Jiaotong University, Xi'an 710049, PR China

[b] State Key Laboratory for Strength and Vibration of Mechanical Structures, School of Aerospace, Xi'an Jiaotong University, Xi'an 710049, PR China

[c] State Key Laboratory for Mechanical Behavior of Materials, Xi'an Jiaotong University, Xi'an 710049, PR China

ARTICLE INFO

Article history:
Available online 28 February 2015

Keywords:
Hybrid
Impact behavior
Concrete
Finite element analysis (FEA)

ABSTRACT

Motivated by the current development trends in the protection fields towards high performance, low cost and lightweight, this study investigates experimentally and numerically the ballistic performance of a novel hybrid-cored sandwich construction: metallic corrugated sandwich plate filled with high performance reactive powder concrete (RPC). Three different types of target plate are fabricated, including monolithic RPC plate, corrugated sandwich directly filled with RPC, and corrugated sandwich with RPC prism insertions and void-filling epoxy resin. The ballistic resistance of each plate vertically penetrated by a projectile at its center is experimentally measured. Numerical simulations with the method of finite elements are subsequently carried out. Corrugated sandwich plate with RPC prism insertions and void-filling epoxy resin achieves the best ballistic performance, as filling the interstices with epoxy resin improves the structural integrity of the sandwich while confinement of the RPC is supplied by the corrugated plates.

1. Introduction

Concrete is widely applied in building as well as protection fields because of its low density (less than 3.0 g/cm^3), low cost, and easy fabrication process. The ballistic performances of normal concrete [1], steel reinforced concrete [2], and fabric jacked concrete [3–5] have been studied extensively. However, the low compressive/tensile strength of traditional concrete structures restrict their application to relatively low velocity impact. In search for high strength concrete (HSC), Bludau et al. [6] demonstrated experimentally that aggregates having higher toughness and hardness led to enhanced ballistic resistance while reactive powder concrete (RPC) invented by the Bouygues Group, which is typically fabricated by mixing silica sand, Portland cement, silica fume, superplasticizer, etc, could achieve a compressive strength exceeding 200 MPa [7], much higher than that of traditional concrete. Subsequently, its was demonstrated that adding steel fibers could increase further the compressive/tensile strength, toughness, and impact resistance of the RPC. Experimentally, Hanchak et al. [8] found that the ballistic resistance of a RPC plate was enhanced as its compressive strength increased, exhibiting shallower penetration depth and smaller crater area relative to traditional concrete plate. Theoretically, Markovich et al. [9] revised the concrete damage model to describe the response of normal concrete under complex loading, while Holmquist et al. [10] put forward a general constitutive model for concrete subjected to large strain, high strain rate, and high pressure. On this basis, Tai [11] carried out numerical studies on the ballistic performance of RPC plates penetrated by flat ended projectiles, and provided a set of parameters for the constitutive model of RPC.

Along a separate research frontier, highly porous all-metallic sandwich constructions with fluid-through cellular cores have emerged as novel lightweight multi-functional structures [12,13]. For instance, in addition to carry structural loads, these sandwich structures can also dissipate heat. The cellular cores exploited thus far are typically periodic, including two-dimensional prismatic cores (e.g., honeycombs and corrugated plates) and three-dimensional lattice truss cores (e.g., pyramidal, Kagome and brazed wire screens). Compared with monolithic plates, metallic sandwich plates have the advantage of lightweight and high stiffness/strength. With good energy absorption capabilities, they can also effectively withstand impact and blast loads [14,15].

More recently, it has been demonstrated, both experimentally and theoretically, that metallic corrugated sandwich plates filled with ceramic insertions outperform the corresponding empty ones

* Corresponding author at: Multidisciplinary Research Center for Lightweight Structures and Materials, Xi'an Jiaotong University, Xi'an 710049, PR China. Tel.: +86 298266 5937; fax: +86 29 83234781.

E-mail address: hyxia0707@mail.xjtu.edu.cn (H.Y. Xia).

http://dx.doi.org/10.1016/j.compstruct.2015.02.059

in terms of ballistic penetration resistance [16–18]. The outstanding ballistic performance of such a hybrid-cored sandwich plate lies in its ability to yaw the projectile and absorb the impact energy through the deformation and failure of the substructures. However, high temperature sintering procedure is typically required to process complex ceramic components, adding considerably the fabrication cost. In comparison, with competitive mechanical performance and low density, RPC can be prepared at room temperature and cast into different shapes. Hence, as a replacement of ceramic, the relatively low-cost RPC and its composite metallic sandwich plates show promising potential for protection applications.

Whereas existing studies on the penetration resistance performance of RPC plates considered mainly monolithic constructions, Remennikov et al. [19] demonstrated that axially-restrained steel–concrete–steel sandwich panels were capable of withstanding blast load or high speed impact. However, the concrete examined in [19] was normal concrete other than RPC. Motivated by the current development trend of high performance, low cost and lightweight in protection fields, the present study aims to investigate, both experimentally and numerically, the ballistic performance of RPC and its composite metallic sandwich structures. In addition to monolithic RPC plates, two different types of sandwich construction are considered: corrugated metallic sandwich plates directly filled with RPC, and corrugated metallic sandwich plates with RPC prism insertions and void-filling epoxy resin. Upon validating the finite element (FE) simulation results with experimental measurements, the ballistic limit velocity, failure mechanisms as well as energy absorption capacity of each target plate are systematically investigated. Under the constraint of same total mass, a preliminary optimization is performed.

2. Fabrication of test specimen and ballistic experiment

2.1. Test specimen

With reference to Fig. 1, three different types of test specimen are fabricated, including monolithic RPC plate (RPC plate), corrugated metallic sandwich plate directly filled with RPC (RPC-Corrugated plate), and corrugated metallic sandwich plate with RPC prism insertions and void-filling epoxy resin (RPC-Corrugated-Epoxy plate). The overall dimensions of the RPC plate are 180 mm × 150 mm × 19 mm, while both the RPC-Corrugated and RPC-Corrugated-Epoxy plates have 180 mm × 150 mm × 17 mm.

The monolithic RPC plate is made from a mixture of six raw materials: 42.5# ordinary Portland cement, silica fume, quartz sand, water reducing admixture (polycarboxylate), brass coated steel fibers (0.18–0.23 mm in diameter, 12 mm in length) and distilled water, with mass proportion of 0.9:0.1:1:0.018:0.083:0.15.

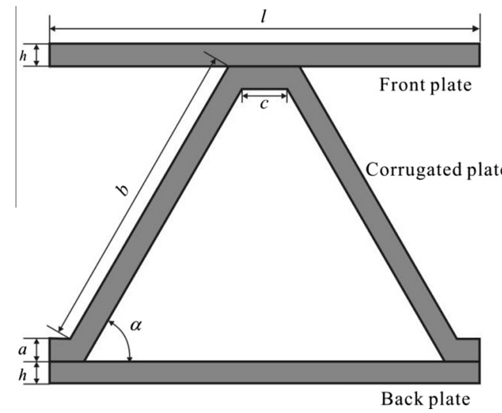

Fig. 2. Schematic of a unit cell of empty corrugated sandwich plate.

After about 3 min of stirring, the mixture is cast into a mould, followed by water oven curing (80 °C for 8 h). The as-fabricated monolithic RPC plate has an areal density of 43.6 kg/m^2, a mass density of 2.29×10^3 kg/m^3 and an axial quasi-static compressive strength of 175 MPa.

To fabricate the RPC-Corrugated and RPC-Corrugated-Epoxy plates, empty corrugated sandwich plates are firstly prepared with AISI 304 stainless steel (with a density of 8.0×10^3 kg/m^3) using the brazing process. Fig. 2 displays the side view of a unit cell of the empty sandwich. The thickness of the front and back face sheets as well as that of the core plate is fixed at $a = h = 1.0$ mm. The corrugated plate has a side length of $b = 18.3$ mm, width of 150 mm, and an inclination angle of $\alpha = 50°$; to facilitate brazing, a small platform of $c = 1.6$ mm is allowed at the apex of the corrugation (Fig. 2).

To fabricate the RPC-Corrugated plate, raw RPC is directly poured into the prismatic voids of the empty sandwich. Upon casting, the RPC-Corrugated plate is placed at room temperature for 24 h and then cured under the same condition as the monolithic RPC plate. The as-fabricated RPC-Corrugated plate has an areal density of 55.4 kg/m^2 and a mass density of 3.26×10^3 kg/m^3.

For the RPC-Corrugated-Epoxy plate, RPC prisms are firstly fabricated following the same procedures as those for the monolithic RPC plate. In order to leave space for epoxy resin, these RPC prisms have slightly smaller transverse dimensions (base 20 mm and height 12 mm) than the prismatic voids of the corrugated plate. Subsequently, epoxy resin is poured into the prismatic voids before the RPC prisms are inserted, with extra epoxy resin extruded out after the insertion is complete. Finally, the hybrid-cored sandwich plate is placed at room temperature for 7 days to solidify the epoxy resin. The as-fabricated RPC-Corrugated-Epoxy plate has an areal density of 50.6 kg/m^2 and a mass density 2.97×10^3 kg/m^3.

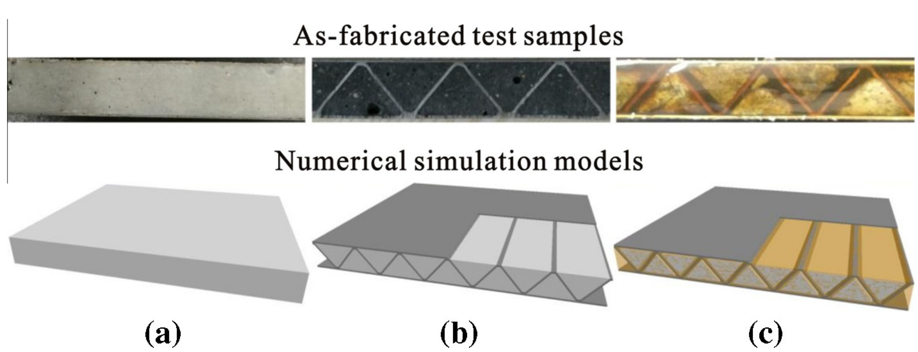

Fig. 1. Comparison between numerical (finite element) model and as-fabricated test sample for protective application: (a) monolithic RPC plate, (b) corrugated metallic sandwich plates directly filled with RPC, and (c) corrugated metallic sandwich plates with RPC prism insertions and void-filling epoxy resin.

2.2. Experimental setup

Each test specimen is vertically penetrated by a hemispherical projectile (6.0 mm in diameter and 15.0 mm in length) at its center, which coincides with the apex of the corrugated plate. The projectile is made from AISI 304 stainless steel, with a total mass of 3.06 g. The same ballistic experiment setup as that described in [18] is employed. Each target plate is fully clamped by a purposely-built target frame. The projectile is launched by a 14.5 mm ballistic rifle, with its initial velocity (ranging from 500~2000 m/s) controlled by gunpowder mass. Timing devices are used to measure the time during which the projectile penetrates through a pair of tinfoil targets placed before and behind the target plate. The velocity of the projectile is calculated by dividing the distance between the tinfoil targets by the measured time. By changing systematically the initial velocity of the projectile, the ballistic limit velocity of each plate is obtained. After the ballistic tests, each target plate is cut with water jet saw to reveal local damage/failure appearances, which are later compared with those simulated numerically.

3. Numerical simulations

3.1. Mesh generation

Numerical models (meshes) are generated using the FE software ANSYS, while numerical calculations are performed with explicit LS-DYNA, both commercially available. The numerical model for each target plate has the same overall dimensions of the test specimen, as shown in Fig. 1. Each model is established using reduced integration solid elements defined by eight nodes having nine degrees of freedom (SOLID 164). To highlight the details of deformation and failure, the region directly under projectile impact is modeled with relatively dense meshes. To balance numerical convergence and computational time, the three different target plates are meshed with 456,000, 658,080, 478,800 elements, respectively, and the projectile is meshed with 5632 elements. Mesh convergence analysis shows that further mesh refinement has little improvement on the accuracy but greater sacrifice of computational time.

3.2. Constitutive models and failure criteria

3.2.1. Steel

The widely applied constitutive model (JC model) of Johnson and Cook [20] for metals subjected to large strain, high strain rate and high temperature is adopted to characterize the material make (304 stainless steel) of empty sandwich plates and the projectile. In the JC model, the yield stress of the material is defined as:

$$\sigma_y = \left(A + B\varepsilon_p^n\right)(1 + C\ln\dot{\varepsilon}^*)(1 - T^{*m}) \tag{1}$$

where A, B, n, C and m are material constants, ε_p is the equivalent plastic strain, $\dot{\varepsilon}^*$ is the normalized strain rate, and T^* is the relative temperature. The failure criterion takes the dependence of deformation process into account by accumulating damage, with the damage of a material element defined as:

$$D = \sum \frac{\Delta\varepsilon}{\varepsilon^f} \tag{2}$$

where $\Delta\varepsilon$ is the increment of equivalent plastic strain in a cyclic integral and ε^f is the equivalent failure strain for the current strain rate, temperature, pressure and equivalent stress.

Typically, the JC model is combined with the Gruneisen equation of state (pressure-specific volume relationship), which defines the pressure as:

$$p = \frac{\rho_0 C^2 \mu\left[1 + (1 - \frac{\gamma_0}{2})\mu - \frac{\beta}{2}\mu^2\right]}{\left[1 - (S_1 - 1)\mu - S_2\frac{\mu^2}{\mu+1} - S_3\frac{\mu^2}{(\mu+1)^2}\right]} + (\gamma_0 + \beta\mu)E \tag{3}$$

for compressible materials and

$$p = \rho_0 C_p^2 \mu + (\gamma_0 + \alpha\mu)E \tag{4}$$

for inflatable materials. Here, $\mu = 1/V - 1, V$ is the current relative volume, C_p is the intercept of the $u_s - u_p$ (shock wave velocity – particle velocity) curve, S_1, S_2 and S_3 are the slopes of the curve, γ_0 is the Gruneisen coefficient, β is the first-order correction of γ_0, and E is the internal energy of the material. Material parameters used in this study for AISI 304 stainless steel are listed in Table 1 [21].

3.2.2. RPC

The general constitutive model (JHC model) put forward by Holmquist, Johnson and Cook [10] is suitable for both normal concrete and RPC subjected to large strain, high strain rate, and high pressure. The JHC model defines the normalized equivalent stress as:

$$\sigma^* = \frac{\sigma}{f_c'} = \left[A'(1 - D) + B'P^{*N}\right][1 - c\ln(\dot{\varepsilon}^*)] \leqslant S_{\max} \tag{5}$$

where σ is the actual equivalent stress, f_c' is the axial quasi-static compressive strength, D stands for accumulated damage, P^* is the normalized pressure, $\dot{\varepsilon}^*$ is the normalized strain rate, A', B', N, c and $S_{\max}$ are material constants, and $S_{\max}$ is the normalized maximum strength. The accumulated damage is defined as:

$$D = \sum \frac{\Delta\varepsilon_p + \Delta\mu_p}{D_1(P^* + T^*)^{D_2}} \tag{6}$$

where $\Delta\varepsilon_p$ and $\Delta\mu_p$ are the equivalent plastic strain increment and plastic volumetric strain increment, respectively, T^* is the normalized hydrostatic pressure, and D_1 and D_2 are material constants. In the JHC model, the relationship between pressure and volume is defined as:

$$P = \begin{cases} K_e\mu, 0 \leqslant P < P_{\text{crush}} \\ P_{\text{crush}} + K_{\text{crush}}(\mu - \mu_{\text{crush}}), P_{\text{crush}} \leqslant P < P_{\text{lock}} \\ K_1\bar{\mu} + K_2\bar{\mu}^2 + K_3\bar{\mu}^3, P \geqslant P_{\text{lock}} \end{cases} \tag{7}$$

where μ and $\bar{\mu}$ are volumetric strain and revised volumetric strain, respectively, and K_e, K_{crush}, K_1, $K_2, K_3, P_{\text{crush}}, \mu_{\text{crush}}$ and P_{lock} are material constants.

As mentioned earlier, the axial quasi-static compressive strength of the present RPC is measured to be 175 MPa, which is similar to that reported by Tai [11]. Consequently, the concrete material parameters used in this study are taken from [11], as summarized in Table 2.

3.2.3. Epoxy resin

As a filling material for bonding between RPC insertions and metal plates, the epoxy resin may be regarded as a kind of hydrodynamic material because of its small amount and low strength. Thus, the constitutive model adopted for epoxy resin is the

Table 1
Material parameters for AISI 304 stainless steel used in JC model and Gruneisen equation of state.

Parameter	Value	Parameter	Value	Parameter	Value
ρ (g cm^{-3})	7.9	G (GPa)	80	A (GPa)	0.31
B	1	n	0.65	C	0.07
m	1	S_1	1.49	S_2	0
S_3	0	γ_0	1.93	C_p (m s^{-1})	4519

Table 2
Material parameters for RPC used in JHC model.

Parameter	Value	Parameter	Value	Parameter	Value
ρ (g cm^{-3})	2.6	G (GPa)	22.8	T (MPa)	13.8
A'	0.79	B'	1.35	N	0.4
c	0.007	f'_c	175.3	S_{max}	3.5
D_1	0.78	D_2	1	ε_p^f	0.0168
P_{crush} (GPa)	0.0584	μ_{crush}	0.0017	P_{lock} (GPa))	0.8
μ_{lock}	0.1				

elastic–plastic-hydro model. Accordingly, the main parameters of epoxy resin used in the current study are: mass density 1.19 g/cm^3, shear modulus 769 MPa, yield stress 70 MPa. This approach has been previously validated by Ni et al. [11] and Lopez-Puente et al. [22].

3.3. Other settings for FE simulations

3.3.1. Fluid–structure interaction

The Lagrange method embedded in the FE code LS-DYNA is employed to describe the movement of structure boundaries. For fluid analysis the Euler method is adopted, as it keeps the meshes undeformed and the material flows among the meshes. Consequently, except for epoxy resin, the substructures of the target plate as well as the projectile are simulated with Lagrange meshes, while the epoxy resin is dealt with Euler meshes. The ALE (Arbitrary–Lagrangian–Eulerian) method is used to handle fluid–structure interaction.

3.3.2. Contact algorithm

Contact surfaces between the projectile and target substructures are defined as surface-to-surface-eroding contact, which describes penetration details by deleting elements according to the failure criterion of the material. For RPC-Corrugated plate, the casting surfaces between the sandwich and the RPC prisms are defined as automatic-surface-to-surface contact, as the effectiveness of this approach was testified by Remennikov and Song [19]. For RPC-Corrugated-Epoxy plate, there is no need to define contact between epoxy resin and substructures since fluid–structure interaction has already been defined. To avoid the overlap phenomenon, the penalty scale factor of contact stiffness is set to be 0.5. Accordingly, a time step scale factor of 0.6 is defined to ensure convergence.

3.3.3. Boundary condition

As a kind of transient incident, localized stress distribution in the target plate appears during the penetration process of the projectile, and there is not enough time for macro deformation of the plate before the projectile penetrates across the structure. As a result, different boundary conditions assigned to the plate have little influence on the results of the FE simulations. In the current study, following Ni et al. [18], clamped boundary conditions are adopted.

4. Comparison between FE simulation and ballistic measurement

For each type of target plate considered, Fig. 3 plots the exit velocity of the projectile as a function of its initial velocity. Overall, good agreement is achieved between measurement and FE simulation. The ballistic limit for the RPC, RPC-Corrugated and RPC-Corrugated-Epoxy plates is approximately 500 m/s, 800 m/s and 1100 m/s, respectively. The ballistic limit is defined as the maximum initial velocity at which the projectile consistently fails to penetrate across the target plate, i.e., its exit velocity is approximately 0.

Fig. 4 compares the experimental observed and numerically predicted local damage (cross-sectional view at the center of each plate) caused by projectile penetration. Here (and in the following sections as well), for clear display of the RPC prisms, the epoxy resin is not plotted for the RPC-Corrugated-Epoxy plate. To reveal more clearly the damage state of the back face, the initial velocity selected is a little higher than the ballistic limit, i.e., 600 m/s for RPC, 900 m/s for RPC-Corrugated, and 1200 m/s for RPC-Corrugated-Epoxy.

It can be seen from Fig. 4(a) that the FE simulations capture the main features of the experimentally observed radial cracks and inverted funnel-shaped damage in the RPC plate. Similar results were reported by Tai [11], using the same concrete material parameters listed in Table 2. As for the sandwich plates, both the deformation pattern of the corrugated metal plates and the fracture pattern of the RPC prisms predicted by FE simulations are also analogous to the experimental ones in Fig. 4(b) and (c). In addition, as observed in the experiments for RPC-filled sandwich plates, large plastic deformation and perforation of the back plate and its peeling-off from the hybrid core also emerge in FE simulations. Nonetheless, the petaloid-shaped torn edges of the back plate shown in Fig. 4(b) and (c) are not totally simulated. This is mainly attributed to the fact that the smashed RPC elements which make no more contribution to ballistic resistance are deleted in numerical simulations whereas these fragments are still present during experiment. However, as demonstrated in Fig. 3, this subtlety has little influence on the prediction of the ballistic limit.

In summary, the agreement between experimental measurements and FE predictions shown in Figs. 3 and 4 in terms of ballistic limit and damage pattern demonstrate the validity of the present numerical approach.

5. Results and discussion

5.1. Comparison with competitive sandwich constructions

Table 3 summarizes the present experimental and numerical results, where ρ_A stands for the areal density, V_e and V_s represent separately the experimentally measured and numerically simulated ballistic limit, and δ denotes the relative error. Without confinement for concrete cracking, the ballistic limit of the RPC plate is as low as about 500 m/s. In comparison, the

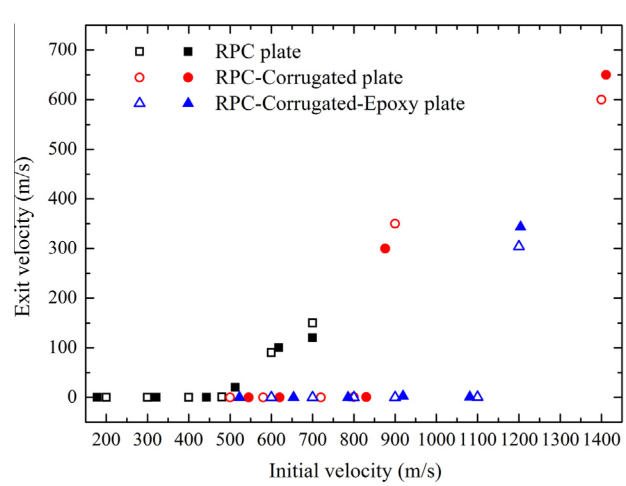

Fig. 3. Exit velocity of the projectile plotted as a function of initial velocity experimentally and numerically (solid dots stand for experimental data, and hollow dots stand for numerical data).

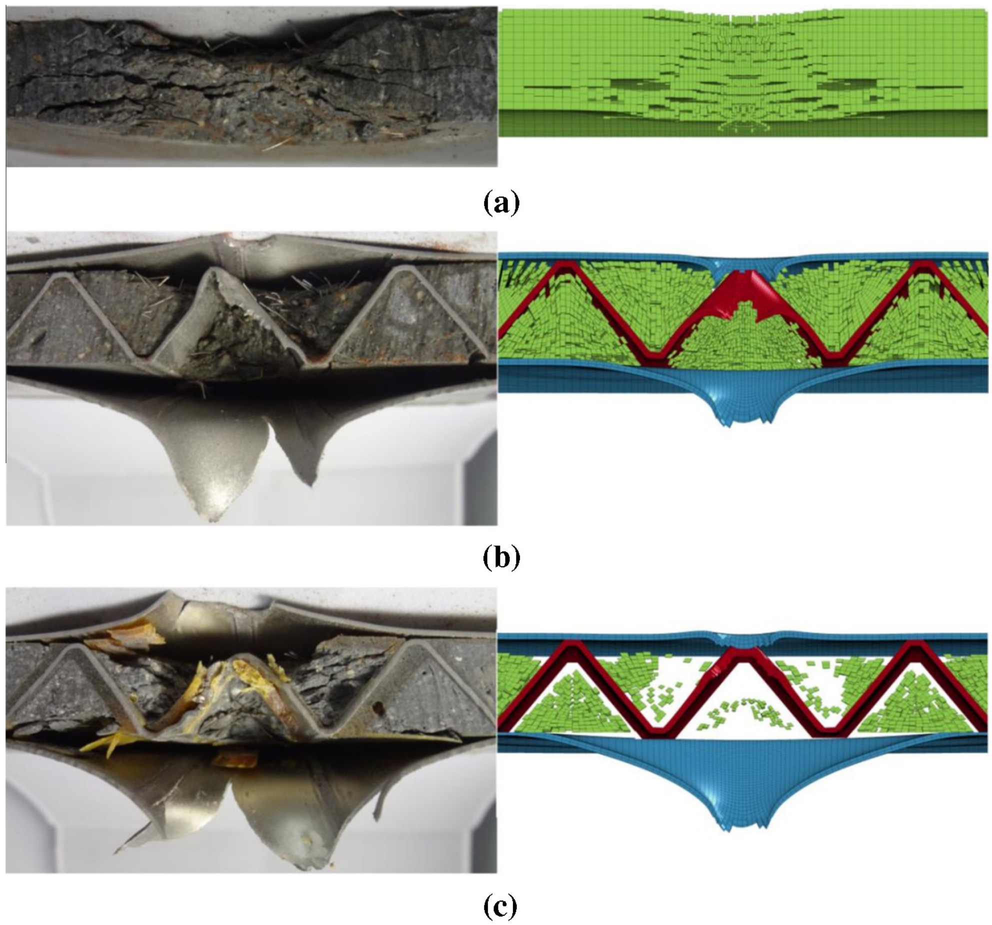

Fig. 4. Comparison of experimental observed and numerically predicted local damage of target plate (cross-sectional view at plate center) after projectile penetration: (a) RPC plate, initial velocity 600 m/s, (b) RPC-Corrugated plate, initial velocity 900 m/s, (c) RPC-Corrugated-Epoxy plate, initial velocity 1200 m/s (epoxy resin not plotted for clarity).

ballistic limit of the RPC-Corrugated plate is increased by ∼63%, accompanied by a moderate increase (27%) in areal density. The RPC-Corrugated-Epoxy plate has the best ballistic performance, as its ballistic limit is about 107% and 27% higher than the RPC plate and the RPC-Corrugated plate, respectively, whereas its areal density is only 16% higher than the RPC. Due to the smaller size of the RPC insertions and the filling of epoxy resin in the interstices between RPC insertions and metal plates, its areal density is even 9% lower than the RPC-Corrugated plate.

For the three different target plates investigated in the present study, Fig. 5 plots their experimentally measured ballistic limit as a function of areal density. For comparison, experimental results obtained by Ni et al. [18] for pyramidal lattice truss core sandwich plates (material make: 304 stainless steel) with and without ceramic (AD 98 alumina) insertions are also included: empty pyramidal sandwich (Pyramidal plate), pyramidal sandwich with ceramic prism insertions (Pyramidal-Ceramic plate), and pyramidal sandwich with ceramic prism insertions and void-filling epoxy resin (Pyramidal-Ceramic-Epoxy plate). Further, for completeness, Fig. 5 also includes the present FE simulation results for a monolithic ceramic (AD 98 alumina) plate and an empty corrugated plate (304 stainless steel).

From Fig. 5 it is seen that an empty steel pyramidal sandwich exhibits superior ballistic resistance relative to a monolithic RPC plate, with only about half of the areal density of the latter. The pyramidal lattice truss core absorbs the impact energy mainly by large bending deflections of the truss members and fracturing at

Table 3
Summary of experimental measurements and FE predictions.

Target plate	ρ_A (g cm^{-2})	V_e (m s^{-1})	V_s (m s^{-1})	δ (%)
RPC plate	4.36	514	500	2.7
RPC-Corrugated plate	5.54	834	800	4.3
RPC-Corrugated-Epoxy plate	5.06	1062	1100	3.6

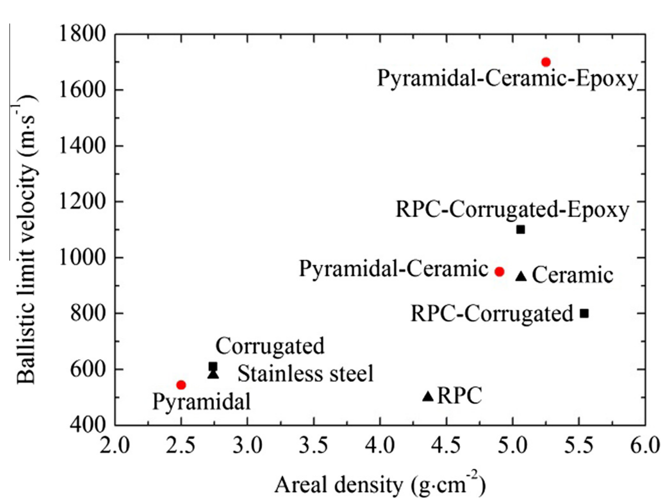

Fig. 5. Ballistic limit velocity plotted as a function of areal density: comparison between the present corrugated-RPC plates and the pyramidal-ceramic plates of Ni et al. [18].

the vertices of the connecting joints. The back face sheet absorbs considerably more energy than the front one, because the projectile that has been slowed down by both the front face sheet and the lattice truss members penetrates through the back face sheet over a much longer time period, inducing not only perforation fracture but also large plastic deformation of the back face sheet.

Pyramidal sandwiches with ceramic insertions and corrugated sandwiched with RPC insertions have similar areal densities, with or without epoxy bonding. Whereas a Pyramidal-Ceramic plate outperforms a RPC-Corrugated plate, its ballistic performance is inferior to a RPC-Corrugated-Epoxy plate; see Fig. 5. Overall, the best performance is achieved by the Pyramidal-Ceramic-Epoxy plate, for two main reasons. Firstly, the ceramic (AD 98 alumina) used by Ni et al. [18] has a compressive strength ($\sim$4 GPa) much higher than that (175 MPa) of the present RPC. Secondly, the ceramic insertions in the Pyramidal-Ceramic-Epoxy plate experiences three-dimensional (3D) network confinement supplied by the pyramidal trusses relative to the two-dimensional (2D) confinement of RPC insertions by corrugated plates.

Although the present RPC-Corrugated-Epoxy plate is not favored against the Pyramidal-Ceramic-Epoxy plate having similar areal density, its potential as a lightweight armor is quite significant and hence should be further explored. Firstly, the cost of RPC fabrication (room temperature casting) is considerably smaller than that (high temperature sintering) of ceramic. Secondly, a pyramidal sandwich plate with RPC casted in situ is expected to perform better than a RPC-Corrugated-Epoxy plate, because the former does not need epoxy resin for bonding as the RPC and the 3D pyramidal trusses form an integrated whole piece. This issue will be addressed in a separate study.

5.2. Analysis of FE simulation results

5.2.1. Evolution of deformation and failure

The evolution of deformation and failure in the RPC, RPC-Corrugated and RPC-Corrugated-Epoxy plates are presented in Figs. 6–8, respectively, at their corresponding ballistic limit velocities. To reveal more clearly the local damage appearance in each plate, the penetrating projectile is removed in these figures. The deformation, erosion and mass loss of the projectile are analyzed separately in the next section.

Fig. 6 shows that the front surface of a monolithic RPC plate is firstly destroyed by the compressive stress induced by the impacting projectile. Subsequently, radial cracks emerge due to the relatively low tensile and shear strength of the RPC compared with its compressive strength. The radial cracks stretch as the projectile continues to penetrate into the interior of the RPC plate. When the compressive stress reaches the back surface and reflects back as a tensile stress, slabbings are formed on the back surface. The final damage appearance of the RPC plate is like an inverted funnel, typical for RPC type material [11]. In conclusion, the low tensile and shear strength of the RPC and the lacking of confinement to the RPC plate result in its poor ballistic performance compared to other competitive structures shown in Fig. 5.

Consider next the RPC-Corrugated plate. Herein, unless otherwise stated, we define the prism directly under projectile impact as central RPC prism, and the remaining prisms as side RPC prisms. It is seen from Fig. 7 that, upon projectile strike, a crater on the front face sheet is formed at first. Once the front face is perforated (via mainly shear-off failure) and the corrugated plates start to deform plastically, the central RPC prism begins to fracture. Subsequently, the corrugated plates experience large plastic deformation and are eventually perforated, causing the side RPC prisms adjacent the central one to fracture. At about 34 μs after the initial strike, the projectile reaches the back face. Thereafter, as 304 stainless steel has good ductility, large deformation of the back face occurs due to bending and stretching. It is worth noting that only the central RPC prism is severely smashed and the 4 adjacent RPC prisms experience large scale fracture. This is because, in the absence of epoxy bonding, the stress generated in the central impact zone cannot spread efficiently to adjacent cells. In other words, whereas the confinement supplied by the folded plates to RPC insertions leads to enhanced ballistic resistance relative to monolithic RPC plate, the enhancement is limited because the integrality of the RPC-Corrugated plate is poor as a result of weak interfacial bonding.

The role of improved interfacial bonding by filling the interstices between RPC insertions and folded metal plates with epoxy resin is explored next for the RPC-Corrugated-Epoxy plate. Fig. 8 demonstrates that the front face and the folded plates in the central impact zone are rapidly perforated at about 12 μs. Because of the high initial velocity (1100 m/s) of the projectile, both experience shear-off failure instead of large plastic deformation. At about 34 μs, in addition to the central RPC prism, severe cracking occurs in as many as 6 adjacent RPC prisms to help absorb the kinetic energy as a result of the significantly improved integrality of the plate. Similar conclusions are reached for metallic pyramidal sandwiches filled with ceramic insertions and epoxy resin [16,18].

5.2.2. Eroding of projectile

To further explore the mechanisms underlying the ballistic performance of the three target plates, Fig. 9 presents the simulated results of the relative length and mass of the projectile, defined here as the ratio of its residual length and mass to initial length and mass, respectively. Upon penetrating across the monolithic RPC plate, the projectile is squeezed into a dumpy shape, but its mass is nearly preserved (i.e., eroding effect of the RPC on the penetrating projectile is small). In comparison, when the projectile

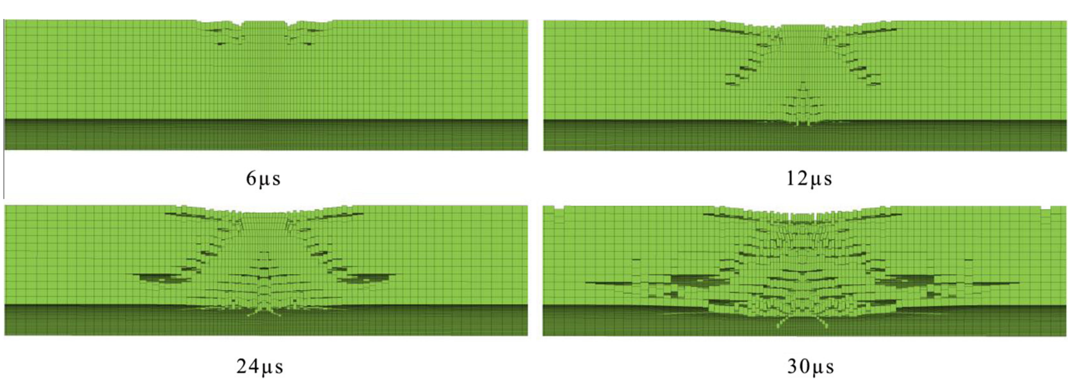

Fig. 6. Evolution of deformation and failure in RPC plate at ballistic limit (500 m/s).

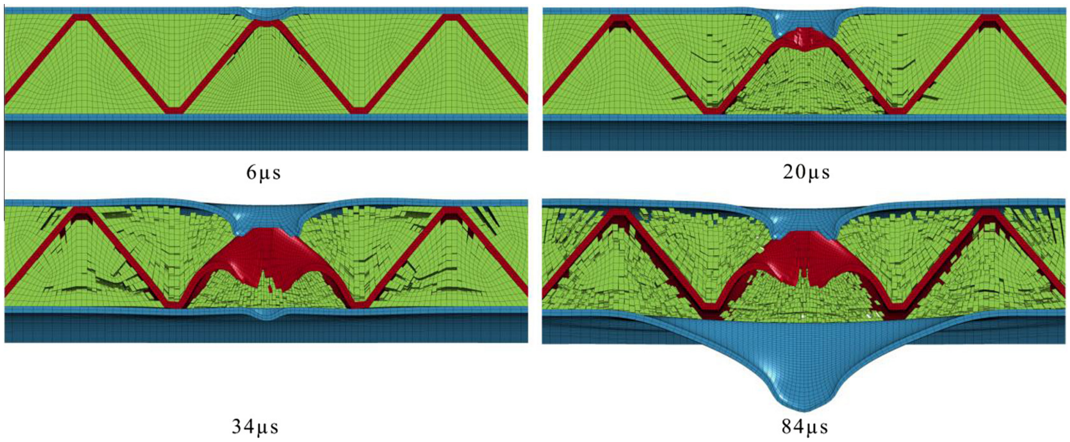

Fig. 7. Evolution of deformation and failure in RPC-Corrugated plate at ballistic limit (800 m/s).

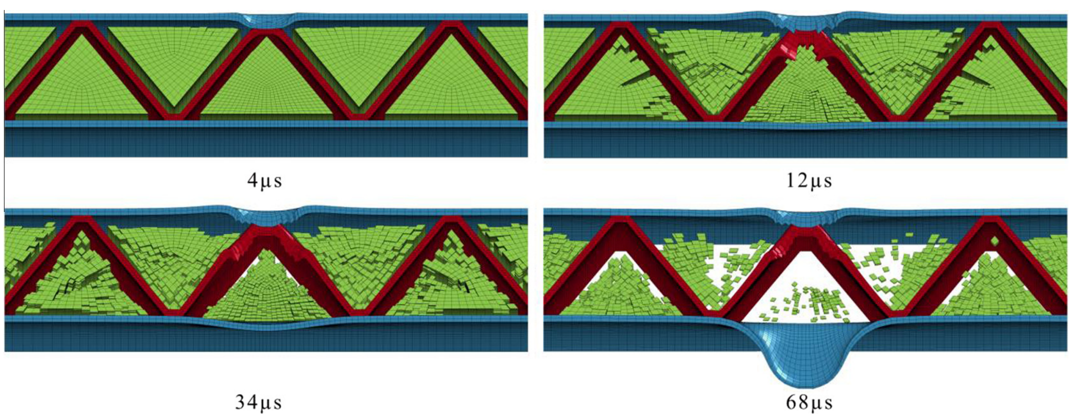

Fig. 8. Evolution of deformation and failure in RPC-Corrugated-Epoxy plate at ballistic limit (1100 m/s).

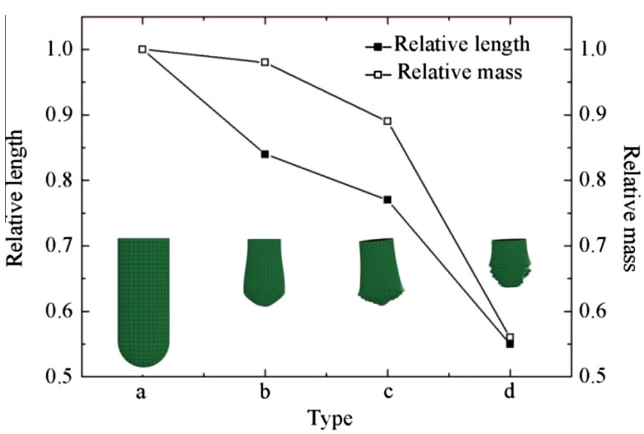

Fig. 9. Appearance of projectile before and after penetration at ballistic limit velocity: (a) before penetration, (b) after penetrating RPC plate, (c) after penetrating RPC-Corrugated plate, (d) after penetrating RPC-Corrugated-Epoxy plate.

penetrates through the RPC-Corrugated and the RPC-Corrugated-Epoxy plates, nearly 10% and 55% of its mass is lost due mainly to erosion, respectively. In addition, during FE simulations, it is observed that the folded plates in both RPC-filled plates cause yawing of the projectile, forcing it to deviate from its ballistic trajectory.

To complement the results of Fig. 9, the projectile velocity is plotted as a function of time in Fig. 10. For the RPC-Corrugated plate, the velocity decreases sharply during the first 20 μs, during which the impact energy is absorbed by plastic deformation of the front face and folded plates as well as fracture of the RPC prisms. From 20 μs to 34 μs, the velocity drop slows down considerably as the projectile is now penetrating through the hybrid core. Afterwards, the projectile contacts with the back face and its velocity decreases sharply again. On the contrary, the velocity versus time curve of the RPC-Corrugated-Epoxy plate is not piecewise before the projectile reaches the back face at 68 μs, and the rate at which the projectile velocity decreases is greater than that of the RPC-Corrugated plate. This suggests that the shear-off failure mode of both the front face sheet and folded plates in the central impact zone together with the large-scale fracture of the epoxy confined RPC prisms (see Fig. 8) act to efficiently decelerate and erode the penetrating projectile.

5.2.3. Energy absorption by substructures

In this section, the amount of energy absorbed by the substructures in RPC-filled sandwich plates is analyzed to explore the role each substructure played during the penetration process. Again, to present the FE simulation results for each target plate, the initial velocity of the projectile is fixed at the corresponding ballistic limit. The absorbed energy discussed here is the summation of internal energy and kinetic energy, with the energy absorbed by the epoxy resin ignored because of its small contribution to total energy absorption. The energy absorption curve of the RPC plate is not presented as it has only one substructure.

For the RPC-Corrugated plate, Fig. 11(a) shows that the energy absorbed by its front face starts immediately after projectile impact, increasing rapidly due to plastic deformation and then

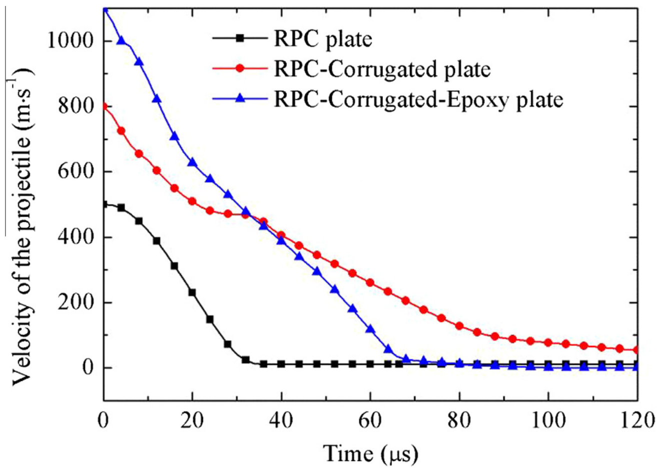

Fig. 10. Velocity of projectile plotted as a function of time at ballistic limit velocity of 500 m/s for RPC plate, 800 m/s for RPC-Corrugated plate, and 1100 m/s for RPC-Corrugated-Epoxy plate.

finishing abruptly at about 10 μs when it is fully perforated. The corrugated plates start to absorb energy slightly after the front face, at an increasing rate similar to the latter, finishing at about 25 μs when those plates in the central zone are perforated as well. Roughly between 25 μs and 35 μs, the impact energy of the projectile is absorbed mainly by the RPC prisms (the central one in particular). However, due to lacking of good confinement to RPC cracking and the considerably lower strength of RPC relative to steel, the RPC prisms absorb only a small amount (<10%) of the total impact energy. Beyond about 35 μs, the remaining impact energy is mainly consumed by the back face via bending and stretching deformation. The contribution of the back face to total energy absorption increases steadily till it is perforated at about 80 μs, reaching a level comparable to that achieved by the corrugated plates. Overall, the corrugated plates play a dominant role in energy absorption for the RPC-Corrugated plate. This is quite different from the ceramic-filled pyramidal sandwich plates [18] where the high strength ceramic absorbs more energy than the pyramidal lattice trusses.

For the RPC-Corrugate-Epoxy plate, the energy absorbed by each substructure is ranked from high to low as follows: corrugated plates, back face, front face, central RPC prism, and side RPC prisms, which is similar to that of the RPC-Corrugated plate. However, relative to the RPC-Corrugated plate, the energy absorbed by the front face is nearly doubled due to the enhancement effect of epoxy bonding, and the energy other substructures

Table 4
Geometrical parameters of RPC-Corrugated-Epoxy plates having same total mass.

Inclination angle α (°)	Fixed face sheet thickness (a)		Fixed core plate thickness (h)	
	b (mm)	h (mm)	a (mm)	b (mm)
30	13.8	1.9	2.6	14.2
40	15.5	1.6	2.0	15.6
45	16.7	1.5	1.6	16.8
50	18.3	1.0	1.0	18.3
60	23.3	0.16	0.15	23.4

absorbed is likewise increased. Further, the back face of the RPC-Corrugate-Epoxy plate begins to absorb energy considerably earlier (10 μs versus 35 μs; see Fig. 11), for two reasons: one is that the projectile velocity is increased and the other is that all the substructures interact with the penetrating projectile as a whole due to epoxy bonding. Also, as a result of the confinement by epoxy bonding, both the central RPC prism and the side RPC prisms absorb considerably more energy, as shown in Fig. 11(b).

5.3. Preliminary optimization

Since the RPC-Corrugated-Epoxy plate (inclination angle fixed at $\alpha = 50°$) exhibits promising ballistic performance, a preliminary optimization with FE simulations is conducted on this type of plate, with focus placed on identifying the optimal inclination angle while keeping the total mass of the plate unchanged. As shown in Table 4, when α is varied, to maintain the same total mass, one can vary either the thickness h of the face sheet (assuming the two face sheets have identical thickness) or thickness a of the corrugated plate. The mass of the void-filling epoxy resin bonding layer is ignored because of its low density and low volume ratio.

Since the ballistic limit of the RPC-Corrugated-Epoxy plate with $\alpha = 50°$ is measured to be about 1100 m/s, the initial velocity is fixed at 1500 m/s in case that the projectile with a smaller velocity may not fully penetrate across the sandwich plates listed in Table 4. The exit velocity of the projectile is adopted thence to evaluate the ballistic performance of these plates, with smaller exit velocity representing better performance. Fig. 12 plots the predicted exit velocity as a function of inclination angle, along with inserts showing the final damage appearance of each plate. It is seen that, by fixing either the thickness of the face sheet or the thickness of the corrugated plate when the inclination angle is varied, in both cases the RPC-Corrugated-Epoxy plate has the best ballistic performance (i.e., smallest exit velocity) at $\alpha = 45°$.

Consider first the sandwich plates with same thickness of corrugated plates. For a sandwich plate with $\alpha = 30°$, even though

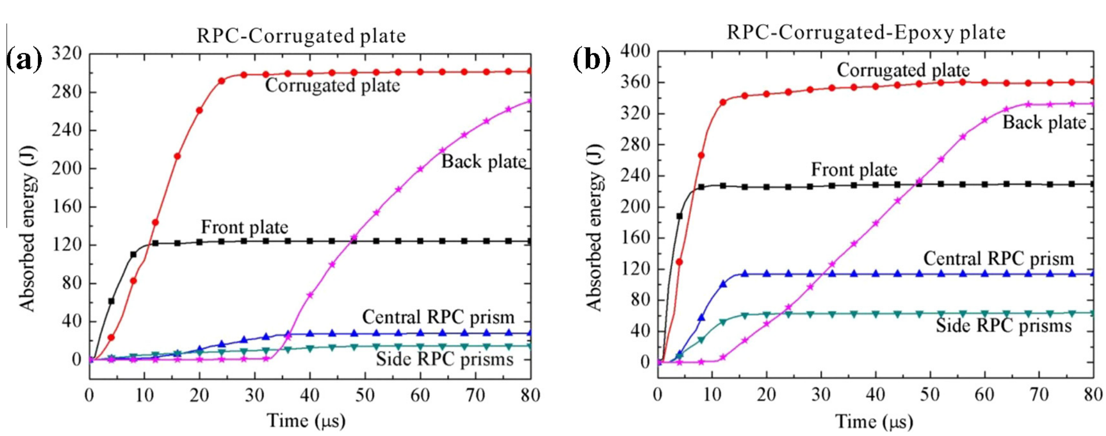

Fig. 11. Energy absorbed by each substructure plotted as a function of time: (a) RPC-Corrugated plate at 800 m/s, (b) RPC-Corrugated-Epoxy plate at 1100 m/s.

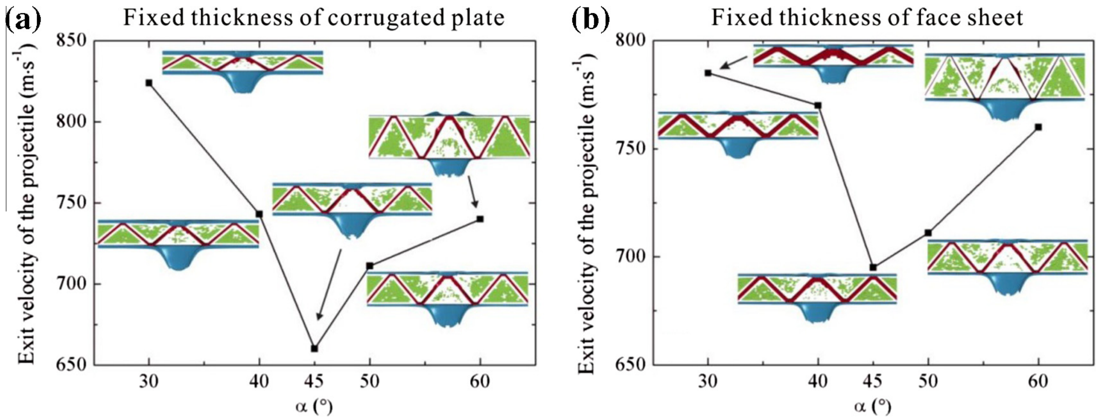

Fig. 12. Exit velocity of projectile plotted as a function of inclination angle for RPC-Corrugated-Epoxy plates having same total mass and: (a) fixed thickness of corrugated plate, (b) fixed thickness of face sheet.

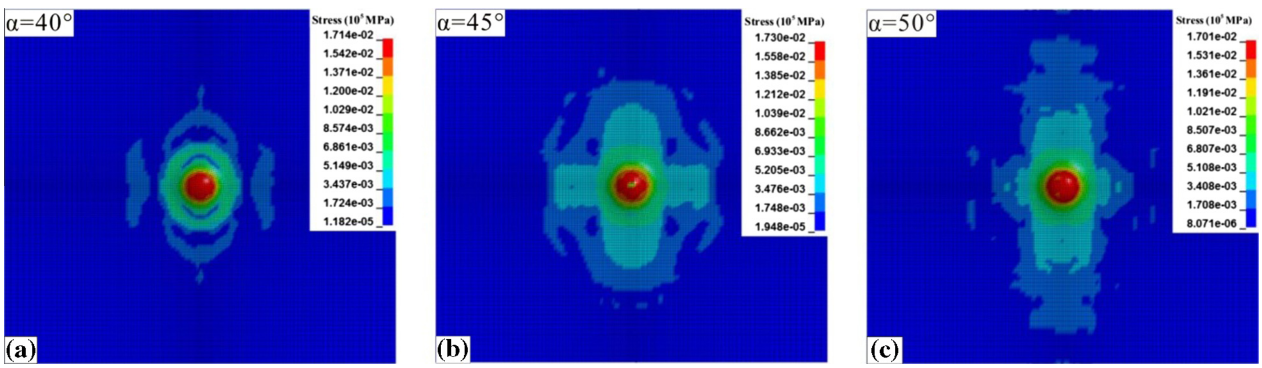

Fig. 13. Distribution of von Mises stress on the back face sheet of RPC-Corrugated-Epoxy plate at the critical time of perforation for: (a) $\alpha = 40°$, (b) $\alpha = 45°$, (c) $\alpha = 50°$.

its face sheets are relatively thick (2.6 mm each), its ballistic performance as shown in Fig. 12(a) is poor because the core height is too thin (14.2 mm) to fully interact with the projectile. Similarly, although a sandwich plate with $\alpha = 60°$ has enough core height, its face sheets are so thin (0.15 mm each) that they cannot fully exploit the shear-off failure process to absorb sufficiently large amount of impact energy. Comparatively, it has been demonstrated that the mechanical properties of an empty corrugated sandwich such as shear/compressive stiffness and strength are optimized if $\alpha = 45°$ [23], which is consistent with the results of Fig. 12. To further explore the underlying mechanism, at the critical time of full perforation, Fig. 13 compares the distribution of von Mises stress on the back face sheet for $\alpha = 40°$, $\alpha = 45°$, and $\alpha = 50°$. It is seen that at the optimal inclination of $\alpha = 45°$ the Mises stress spreads to a broader area (covering three cells), whereas the stress spreading is less effective (restricted mainly to a single cell) when $\alpha = 40°$ or 50°.

As the inclination angle is varied, similar conclusions are obtained for sandwich plates having the same face sheet thickness. The exit velocity is minimized when $\alpha = 45°$. Increasing the corrugated plate thickness reduces the core height, so the $\alpha = 30°$ configuration has poor performance. Note that when $\alpha = 60°$, even

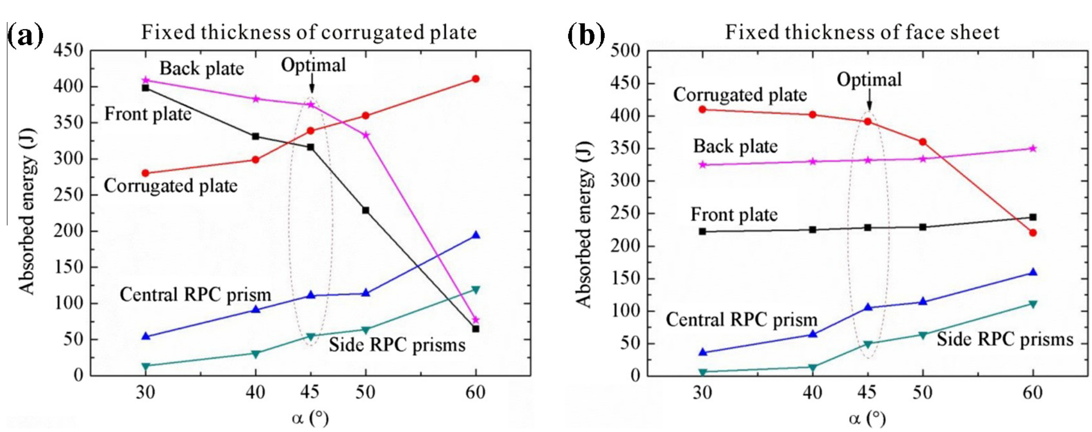

Fig. 14. Absorbed energy of each substructure plotted as a function of inclination for RPC-Corrugated-Epoxy plates having same total mass and: (a) fixed thickness of corrugated plate, (b) fixed thickness of face sheet.

though the corrugated plate is too thin (0.16 mm) to supply enough support for the face sheets, the sandwich structure is not collapsed under projectile impact owing to the confinement supplied by epoxy bonding.

For the two groups of sandwich plates listed in Table 4 and Fig. 14 plots the energy absorbed by each substructure as a function of inclination. It can be seen from Fig. 14(a) that changing the geometrical configuration of the sandwich plates having same corrugated plate thickness would significantly influence the energy absorption capacity of each substructure. Within the range of inclination considered (30–60°), as α is increased, the corrugated plate absorbs more energy although its thickness remains unchanged whereas the face sheets absorb less energy. The energy absorbed by both the central and side RPC prisms also increases steadily with increasing α. When α is less than 45°, the face sheets (the back one in particular) dominate the energy absorption. When $\alpha = 45°$, the energy absorbed by the corrugated plate is increased to a level comparable to that of the face sheets. As α is further increased, the energy absorption capacity of both face sheets decreases rapidly; see Fig. 14(a). Overall, the total energy absorbed by the substructures is maximized when $\alpha = 45°$ and, correspondingly, the sandwich plate with $\alpha = 45°$ exhibits the best ballistic performance.

In contrast, for the sandwich plates with identical face sheet thickness, it is seen from Fig. 14(b) that the corrugated plate rather than the face sheets dominates energy absorption when $\alpha < 45°$. As α is increased, the energy absorbed by both face sheets increases, albeit slightly, because of their constant thickness. The absorbed energy of the corrugated plate also changes little when α is increased from 30° to 45°, because the improvement in energy absorption capacity is counteracted by decreased thickness of the corrugated plate. When α is increased to the optimal angle of 45°, there is an obvious increment in the absorbed energy of the RPC prisms while the energy absorbed by other substructures remains almost unchanged. As α is further increased to 60°, the capacity of the corrugated plate to absorb energy is reduced significantly because its thickness becomes too thin. Correspondingly, the ballistic performance of the sandwich is also poor.

6. Conclusions

The potential of combining reactive powder concrete (RPC) with corrugated metallic sandwich plates for ballistic protection has been investigated experimentally and numerically. The ballistic performances of three different target plates are compared, including monolithic RPC plates, corrugated sandwich plates directly filled with RPC, and corrugated sandwich plates with RPC prism insertions and void-filling epoxy resin. Good agreement is achieved between experimentally measured and numerically simulated results.

Overall, corrugated sandwich plates with RPC prism insertions and void-filling epoxy resin exhibits the best ballistic performance, with only a moderate increase in areal density. Plastic deformation and shear-off failure of the metallic plates as well as cracking and fracture of the RPC prisms combine to absorb the kinetic energy of the projectile. Confinement of RPC supplied by the corrugated plates and improved structural integrity due to epoxy bonding also contribute significantly to enhance the ballistic resistance.

Varying the topological configuration of the RPC-Corrugated-Epoxy plate and the mass distribution of its substructures has great influence on its ballistic performance. Under the constraint of same total mass, the sandwich plate having 45° inclination exhibits the best ballistic performance: balanced mass distribution on the substructures ensures not only adequate core height but also enough thickness of both the face sheets and the corrugated plates, thus the energy absorption capacity of every substructure is fully exploited.

Acknowledgments

This work is financially supported by the National Basic Research Program of China (2011CB6103005), the National 111 Project of China (B06024) and the National Natural Science Foundation of China (11021202, 11072188, 11102152).

References

[1] Frew DJ, Forrestal MJ, Cargile JD. The effect of concrete target diameter on projectile deceleration and penetration depth. Int J Impact Eng 2006;32(10):1584–94.
[2] Kamal IM, Eltehewy EM. Projectile penetration of reinforced concrete blocks: test and analysis. Theoret Appl Fract Mech 2012;60(1):31–7.
[3] Vossoughi F, Ostertag CP, Monteiro PJM, et al. Resistance of concrete protected by fabric to projectile impact. Cem Concr Res 2007;37(1):96–106.
[4] Jacobs MJN, Van Dingenen JLJ. Ballistic protection mechanisms in personal armor. J Mater Sci 2001;36(13):3137–42.
[5] Lam L, Teng JG, Cheung CH, et al. FRP-confined concrete under axial cyclic compression. Cement Concr Compos 2006;28(10):949–58.
[6] Bludau C, Keuser M, Kustermann A. Perforation resistance of high-strength concrete panels. Am Concr Inst Struct J 2006;103(2):188–95.
[7] Richard P, Cheyrezy M. Composition of reactive powder concretes. Cem Concr Res 1995;25(7):1501–11.
[8] Hanchak SJ, Forrestal MJ, Young ER, et al. Perforation of concrete slabs with 48 MPa (7 ksi) and 140 MPa (20 ksi) unconfined compressive strengths. Int J Impact Eng 1992;12(1):1–7.
[9] Markovich M, Kochavi E, Ben-Dor G. An improved calibration of the concrete damage model. Finite Elem Anal Des 2011;47(11):1280–90.
[10] Holmquist TJ, Johnson GR, Cook WH. A computational constitutive model for concrete subjected to large strains, high strain rates, and high pressures. In: 14th International symposium on ballistics, vol. 9; 1993. p. 591–600.
[11] Tai YS. Flat ended projectile penetrating ultra-high strength concrete plate target. Theoret Appl Fract Mech 2009;51(2):117–28.
[12] Wadley HNG. Cellular metals manufacturing. Adv Eng Mater 2002;4(10):726–33.
[13] Wadley HNG, Fleck NA, Evans AG. Fabrication and structural performance of periodic cellularmetal sandwich structures. Compos Sci Technol 2003;63(16):2331–43.
[14] Hutchinson JW, Xue Z. Metal sandwich plates optimized for pressure impulses. Int J Mech Sci 2005;47(4–5):545–69.
[15] Deshpande VS, Fleck NA. One-dimensional response of sandwich plates to underwater shock loading. J Mech Phys Solids 2005;53(11):2347–83.
[16] Wadley HNG, Dharmasena KP, O'Masta MR, et al. Impact response of aluminum corrugated core sandwich panels. Int J Impact Eng 2013;62:114–28.
[17] Yungwirth CJ, O'Connor J, Zakraysek A, et al. Explorations of hybrid sandwich panel concepts for projectile impact mitigation. J Am Ceram Soc 2011;94(S1):62–75.
[18] Ni CY, Li YC, Xin FX, et al. Ballistic resistance of hybrid-cored sandwich plates: numerical and experimental assessment. Compos A 2012;46:69–79.
[19] Remennikov AM, Kong SY. Numerical simulation and validation of impact response of axially-restrained steel–concrete-steel sandwich panels. Compos Struct 2012;94(12):3546–55.
[20] Johnson GR, Cook WH. A constitutive model and data for metals subjected to large strains, high strain rates and high temperatures. In: Proceedings of the 7th international symposium on ballistics, vol. 547, No. 11; 1983. p. 541–47.
[21] Mori LF, Lee S, Xue ZY, et al. Deformation and fracture modes of sandwich structures subjected to underwater impulsive loads. J Mech Mater Struct 2007;2(10):1981–2006.
[22] Lopez-Puente J, Arias A, Zaera R, et al. The effect of the thickness of the adhesive layer on the ballistic limit of ceramic/metal armors: an experimental and numerical study. Int J Impact Eng 2005;32(1–4):321–36.
[23] Kazemahvazi S, Zenkert D. Corrugated all-composite sandwich structures. Part 1: Modeling. Compos Sci Technol 2009;69(7):913–9.